A fast one-pot synthesize of crystalline anglesite by hydrothermal synthesis for environmental assessment on pure phase

Matthias Monneron–Gyurits, Emmanuel Joussein, Alexandra Courtin-Nomade, O. Grauby, Erwan Paineau, Solenn Reguer, Marilyne Soubrand

A fast one-pot synthesize of crystalline anglesite by hydrothermal synthesis for environmental assessment on pure phase

Matthias MONNERON--GYURITS [a], Emmanuel JOUSSEIN [a], Alexandra COURTIN-NOMADE [a,b], Olivier GRAUBY [c], Erwan PAINEAU [d], Solenn REGUER [e], Marilyne SOUBRAND [a]

[a] Université de Limoges, PEIRENE-EAU EA 7500 E2LIM, 123 avenue Albert Thomas, 87060 Limoges Cedex, France

[b] Université Paris Saclay, Géosciences Paris Sud GEOPS UMR CNRS-UPS 8148, rue du Belvédère Bâtiment 504, 91400 Orsay, France.

[c] Centre Interdisciplinaire de Nanoscience de Marseille (CINaM), CNRS/Aix-Marseille Université, Campus de Luminy, 13288 Marseille, France.

[d] Laboratoire de Physique des Solides, UMR CNRS 8502, Université Paris-Saclay, 1 rue Nicolas Appert, Bâtiment 510, 91405 Orsay Cedex, France.

[e] DIFFABS Beamline, Synchrotron SOLEIL, L'Orme des Merisiers Saint-Aubin, BP 48 91192 Gif-sur-Yvette Cedex, France.

* Corresponding author. Emmanuel JOUSSEIN, Université de Limoges, FST, E2LIM PEIRENE EAU EA 7500, 123 avenue Albert Thomas, 87060 Limoges, France. Mail. emmanuel.joussein@unilim.fr

Submitted to ESPR

Abstract

Anglesite ($PbSO_4$) is a lead sulfate that belongs to the barite group and is naturally ubiquitous in the environment. This work describes a simple way to synthesize crystalline lead sulfate by using a straightforward hydrothermal procedure. Typically, $Pb(NO_3)_2$ and $Fe_2(SO_4)_3$ precursors were mixed and heated at 94°C for 24h. The synthesized samples have been characterized by coupling X-Ray diffraction (XRD) to spectroscopic methods (FTIR and micro-Raman), X-ray absorption spectroscopy (XAS) and electronic microscopy (SEM and TEM). *In fine*, the results about this new well crystalline synthetic anglesite confirm the efficiency and the importance of this cheap protocol and the synthesized phases obtained. Moreover, the environmental stability and bioaccessibility of anglesite has been done to evaluate environmental stability of anglesite

under various physico-chemical conditions and sanitary risks. Finally, the paper allows to obtain precise data on a pure phase in order to be able to more easily evaluate and understand the role of anglesite in As-polluted sites and soils.

Keyword: hydrothermal synthesis, anglesite, characterization, spectroscopy, morphology, environmental stability.

Introduction

Anglesite ($PbSO_4$) is a natural lead sulfate, described for the first time in 1783 by William Withering (Zeman 1950). This mineral belongs to the barite group with a general formulation $A(SO_4)$, where A may be Pb^{2+}, Ba^{2+}, Sr^{2+} or Cr^{2+}. The divalent atoms are 12-coordinated to isolated SO_4 groups, which form regular tetrahedron. Their structures were first determined by James and Wood (1925) indicating an orthorhombic form with the space group *Pnma*.

Anglesite is a typical oxidation by-product of galena (PbS) within lead ore deposits in supergene environment (i.e. Boni et al., 2003; Mondillo et al., 2014) and is widely observed in Pb-mining contexts as nanoparticles (e.g. Courtin-Nomade et al. 2016; Frau et al. 2009; Hayes et al. 2012). In the environment, lead is known for its significant toxicity; the awareness of the behavior of its different bearing phases thus appears to be a major health risk during ingestion or inhalation (Pascaud et al. 2014). Since a lot of Pb-contaminated SUITMA (Soils of Urban, Industrial, Traffic, Mining and Military Areas) are effective worldwide, it is of prime importance to estimate the potential contribution of anglesite, a ubiquitous mining waste phase, in such contaminated soils regarding potential sanitary risks as well as its behavior toward ingestion. However, soil is well known to be a complex material due to the heterogeneity of its composition in terms of chemical and mineralogical point of view, usually constituted of multi-phases [*e.g.* quartz, feldspars, clay minerals and various metal(loïd)s bearing phases in a same sample]. It is thus necessary to simplify this system in the way to better understand the contribution of each mineral phases regarding their geochemical behavior or environmental impact. In particular, what is the human sanitary risks contribution of anglesite from contaminated soils? Therefore, the use of mineral synthesis is essential to obtain a pure product, well characterized and as close as possible to the environmental phases. Indeed, the use of pure phases is crucial in the environmental sciences, especially for a better understanding of the sanitary impact related to the stability of anglesite in this case (Monneron--Gyurits et al. 2020). Indeed, it is necessary to carry out specific tests on synthesized phases in order to estimate its behavior over time, to know what controls its dissolution or stability (Pb release or not in human

bodies) and ultimately the crystallo-chemical effects when such (nano)particles are ingested or inhaled into the human body.

In the literature, the protocols for synthesizing Pb phases are rarely or never explored, particularly that of anglesite. The few protocols (Blount 1974; Wang et al. 2001; Xiang et al. 2005; Han et al. 2012) are based on Na_2SO_4 or CS_2 as the sulfur source. Moreover, these protocols often imply laborious, and/or uneconomic experimental procedure either by using high synthesis temperatures ~~(~~[two-step process with calcination at T = 600°C~~)~~ (Han et al. 2012; Wang et al. 2001) or long time synthesis up to 7 days (Xiang et al. 2005)]. To overcome these drawbacks, our study aims to propose a new protocol, easy to set up, to achieve pure crystalline anglesite by soft hydrothermal synthesis in 1 day. The quick set-up of anglesite synthesis in controlled conditions also represents a definite advantage in terms of various study for example to get a sequence of different crystallite sizes, from micro- to nanoscale and to obtain new thermodynamic and crystallographic data. Moreover, this type of sample may be used as standard for various implementation and experiments typically for beamline database. To allow a large number to apprehend the sanitary risks and especially to better reposition the role of anglesite in environmental problems since this mineral is ubiquitous in polluted sites and soils, the environmental stability of anglesite according to BCR and bioaccessibility (UBM protocols) experiments has also been realized.

Material and Methods

Synthesis experiment of anglesite

Lead nitrate ($Pb(NO_3)_2$), iron sulfate ($Fe_2(SO_4)_3$) and 5% ammonium acetate were purchased from Sigma Aldrich with an analysis grade quality (purity > 99%). A new synthesis way of anglesite has been explored using the following protocol: 15g of $Pb(NO_3)_2$ used as Pb^{2+} source and 6.95g of $Fe_2(SO_4)_3$ for the sulfate (SO_4^{2-}) source were weighted in two different polystyrene dishes and directly mixed in same flat-bottom Teflon bomb reactor.

The mixing process were realized under magnetic stirring at 50 rpm. Then, 50 mL of ultrapure water (UPW) produced by a Gradient A10 Milli-Q system (18.2mΩ) from Millipore (Bellerica, MA, USA) was added to the previous mixture and mixed under magnetic stirring rotating at 110rpm for 10min to obtain a good homogenization. The pH value of the solution should be stabilized at 1 (± 0.1 pH unit) before sealing the Teflon bomb reactor by adjusting it from dropwise addition of HNO_3 1M or NaOH 1M under continuous stirring. Finally, the autoclave is placed in a Memmert UN30 oven pre-heated at 94°C. After 24h, the Teflon bomb reactor was slowly cooled at ambient temperature (20°C) for 30min to bring the pressure inside the

reactor to ambient value before opening. The same experiment was also performed during 48h of ageing. Then, the solid was separated from the solution by using cellulose paper filter (Fisherbrand, grade quality 122) and washed sequentially 5 times with UPW (100mL) and 5% ammonium acetate to eliminate the excess of ferric sulfate ~~(~~[$Fe_2(SO_4)_3$]~~)~~]. The last washing was performed with 200mL of ultrapure water. Finally, the solid was placed in a glass vessel and dried in an oven pre-heated at 40°C for 24h until the mass does not vary between two weightings spaced by 2h.

Analytical Methods

X-ray diffraction (XRD), Fourier Transform Infrared spectroscopy (FTIR) and micro-Raman investigations were performed at the CARMALIM analytical platform (CEC, Limoges, France). The structural characterization was performed using XRD analysis. Experiments from powder sample were carried out on a Bruker D8 advance diffractometer at the CuKα wavelength ($\lambda_{K\alpha}$=0.1541 nm), between 5 and 65° 2θ with a 0.04° 2θ step and a counting time of 2 seconds/step. Prior to XRD experiments, the sample was gently grounded using a non-amorphizer ball mill in zirconium oxide (Pulverisette 23, Fritsch). The obtained XRD patterns were processed using EVA software (Bruker). Rietveld analysis was performed from the method implemented in Profex BGMN software (Doebelin and Kleeberg 2015). Drawing of the resulting structure was performed using VESTA software (Momma and Izumi 2011).

FTIR was performed on a Perkin Elmer FT-IR/NIR Frontier Spectrometer device operating in Attenuated Total Reflectance (ATR mode), *i.e.* directly without further preparation, nor KBr pellets. The ATR measurement was performed on powders in the mid infra-red region (600 - 4000 cm^{-1} range) at 2 cm^{-1} resolution for 15 scans.

A Jobin Yvon 6400 was used to perform the Raman spectroscopic analysis. The sample was gently crushed and placed onto a glass chip. A 514nm Argon laser with an incidence power limited at 5mW to avoid any destruction of the analyzed material was used as excitation source. The analysis was performed using a ×50 objective at room temperature from 100 to 1250 cm^{-1} analytical region. Three different windows with an acquisition time ranging from 30s to 200s and three iterations were used in the way to obtain a perfect sensibility and Raman resolution.

The microscopic investigations were done at CINaM/Aix-Marseille University, France. The morphology of anglesite was performed by Scanning Electron Microscopy (SEM) observations with a JEOL 6320 F operated at 15 kV and at low voltage 1kV. Samples were coated with carbon prior analysis. JEOL JEM 2011 Transmission Electron Microscope (TEM) working at 200 kV was also used. The parameters were 50000× magnification, 20° tilt angle toward the EDX detector, energy range of 40 keV, corrected counting time of 30 s, constant beam density

137 ~63.5 pA.cm^{-2}. Elements were quantified using the Bruker AXS TEM line mark data semi-
138 quantification procedure (Berthonneau et al. 2014). EDX chemical analyses were performed on
139 20 individual particles. The size of the particles was manually measured on micrographs using
140 ImageJ software.
141 The local structure of synthetic anglesite was investigated by X-ray Absorption Spectroscopy
142 experiments at the Pb LIII-edge (E0=13035eV) on the DIFFABS beamline (synchrotron
143 SOLEIL, France). The X-ray beam was monochromated with a Si(111) double crystal with a
144 beam focalization assured by Kirkpatrick-Baez mirrors. The energy range was selected between
145 13000 and 13200eV with an energy step of 0.3eV. XANES spectrum was calibrated with a
146 metallic Pb foil at the Pb L-edge (13035keV). Anglesite sample was transferred in a borosilicate
147 capillary before analysis in fluorescence mode using a 4-elements silicon drift detector (Vortex-
148 ME4®). The XANES spectrum was obtained after standard procedures for pre-edge subtraction
149 and normalization using ATHENA software package (Ravel & Newville, 2005). EXAFS data
150 analysis was achieved by fitting the Fourier transformed experimental data with simulations
151 performed with the IFEFFIT code (Ravel & Newville 2005) based on the crystallographic
152 structure obtained from Rietveld refinement.
153 Sequential extractions were realized according to the Commission of the European
154 Communities Bureau of Reference (BCR) protocol (Auret et al. 1999) using a microwave
155 modified procedure (Pérez-Cid et al. 1998). The detailed protocol can be found in **Table SI1**.
156 Briefly, 0.5 g of anglesite was successively mixed with 0.11 M of acetic acid (purity > 99%)
157 (F1 step corresponding to the acid-soluble/exchangeable fraction); 0.10 M of
158 hydroxylammonium (purity > 98%) at pH 2 (F2 step i.e. the reducible fraction relative to metal
159 bound to oxyhydroxides of iron and manganese); and 30% hydrogen peroxide (purity 32%) and
160 1 M ammonium acetate (purity > 98%) at pH 2 (F3 step i.e. the oxidizable fraction
161 corresponding to contaminants associated to organic matter or in sulfide form). After each step,
162 centrifugation (3300*g* for 15 min) was done, and the supernatant recover after 0.45 µm filtration
163 previous Pb analysis.
164 Bioaccessibility tests were performed to assess anglesite behavior in human gastro-intestinal
165 tract in the way to simulate the human physicochemical conditions (pH, temperature, contact
166 time, L/S ratio, and chemical composition) during anglesite accidental ingestion using the
167 unified BARGE protocol (UBM; Denys et al. 2009) since this protocol has been validated from
168 *in vivo* tests for Pb. Briefly, 0.6 g of anglesite were subjected to the gastric extraction (saliva +
169 gastric fluid; L/S = 37.5) and then to gastro-intestinal extraction (saliva, gastric fluid, bile,
170 duodenal fluid; L/S = 37.5) to highlight the difference between gastric and gastro-intestinal

bioaccessibility. The **Table SI 2** summarized the procedure details. The bioaccessibility results is calculated along percentage of total element content.

After BCR and UBM extractions, Pb contents in solution were analyzed by Atomic Absorption Spectrometry using a spectrometer Variant 220FS (FAAS) with a quantification limit for Pb of 0.5 mg L. Pb standards of 1 g L were used for calibration (Certipur Merck), and the BCR-483 sewage sludge-amended soil (trace elements) are used in the way to validate the analyses. All the analysis were conducted in duplicate.

Results and discussion

Time synthesis, purity and processing

The X-ray diffraction pattern of as-synthesized material is presented in **Fig. 1**. Indexation of all peaks is consistent with orthorhombic crystalline anglesite (JCPDF 01-089-7356) with the main peaks located at 20.81, 26.73 and 29.70°2θ. Analysis of the XRD pattern also indicates that our synthetic sample has a high degree of purity without by-products, such as plumbojarosite, ferric sulfate or amorphous phases. Assuming a complete conversion of precursors as ionic forms in liquid phase (the Solubility Product Constants (Ksp) of involved lead sulfate salt at normal conditions for $PbSO_4$ is $K_{sp} = 1.6\times10^{-8}$ from database WATEQ4F (Ball & Nordstrom 1991), then the chemical reaction (**Eq. 1)** can be written simply as:

Eq. 1 Pb^{2+} (aq) + SO_4^{2-} (aq) $\overset{24h}{\Longrightarrow}$ $PbSO_4$ (s)

Beyond a fast synthesis process, another benefit of the proposed protocol is that the mass yield of the reaction is close to 55% after washing. Note that after 48h of hydrothermal treatment (**Fig. SI 1**), some additional reflection arising from impurities of plumbojarosite (JCPDF 00-039-1353) are detected at 14.42, 29.09 and 34.41°2θ. The resulting chemical reaction is the continuity of **Eq. 1** and can be written according to the following **Eq. 2**:

Eq. 2 $3/2Pb^{2+}$ (aq) + $3Fe^{3+}$ (aq) + $3SO_4^{2-}$ (aq) + $6OH^-$ (aq) $\overset{24h\ more}{\Longrightarrow}$ $PbSO_4$ (s) + $Pb_{0.5}Fe_3(SO_4)_2(OH)_6$ (s)

This reaction (**Eq. 2**) is due to (i) the simultaneous presence of $PbSO_4$ and $Fe_2(SO_4)_3$ during the reacting process (Dutrizac et al. 1980) and to (ii) the change of the Eh (redox potential) conditions during time synthesis. Indeed, according to the Eh–pH diagram for part of the system S-O-Fe-Pb-H_2O (*e.g.* Forray et al. 2010; **Fig. SI 2**), the stability domain (Eh-pH) of anglesite in acidic condition is limited. The variation of the pH and Eh values has been measured along 48h, the results evidence that (i) a small decrease of pH value from 0 to 48h inducing a loss of

0.2 unit pH (0.9 to 0.7), and (ii) a slight increase of the Eh value is noted (increase of 100 mV from 24 (500 mV) to 48h (600mV), probably due to the effect of plumbojarosite nucleation/growth. This is clearly enough to get out of the stability range of the anglesite and therefore closer to that of the plumbojarosite. Consequently, up to 24 hours, the conditions of nucleation/growth of the anglesite are optimal but induces a slight physico-chemical modification of the system, favoring the subsequent precipitation of plumbojarosite to the detriment of the anglesite. Note that this hydrothermal synthesis mode is interesting because it is possible to obtain easily reproducible properties and structural characteristics of anglesite. Moreover, it can be possible to control both the size and the crystallinity of the samples which is a significant plus. Accordingly, sample synthesized after 24 h is the one that has been characterized precisely characterize using multi techniques approach described above.

Structural characterization of pure synthesized anglesite

Rietveld experiment has been performed in the way to obtain structural cell parameters of the synthetic samples. The structural characterization is well reproduced with the orthorhombic *Pbnm* Z = 4 structure of anglesite. The lattice parameters of the obtained $PbSO_4$ unit cell are reported in the **Table 1** (a = 6.95225 Å, b = 8.47558 Å, c = 5.39800 Å) and are in accordance with conventional parameters of anglesite found in the literature on both synthetic (Antao 2012) or natural phases (Jacobsen et al. 1998). Finally, the structure parameters determined from Rietveld refinement are presented in **Table 2** and the corresponding 3D structure is reported in **Fig. 2**.

Spectroscopic investigations by coupling FTIR, Raman and XANES measurements are reported in **Fig. 3a** and **3b**, respectively. Firstly, it seems that there is no real difference between reference data from literature and the synthesized one relative to the morphology of the spectra. The characteristic bands of anglesite are only presented between 600 cm^{-1} and 1400 cm^{-1} in the FTIR spectrum (**Fig. 3a**). The sharp band at 625 cm^{-1} is related to the stretching vibration bands ν_4 (SO_4^{2-}) while the bands located at 965 cm^{-1}, 993 cm^{-1} and 1166 cm^{-1} are respectively attributed to ν_1, ν_3 and ν_3 modes of (SO_4^{2-}) (Farmer 1977; Lane 2007). The Raman spectrum (**Fig. 3b**) highlights seven main bands located at 1155, 1060, 973, 640, 605, 449, 438, which can be assigned to ν_3, ν_3, ν_1, ν_4, ν_4, ν_2, ν_2 (SO_4^{2-}) respectively and 132 cm^{-1} to lead sulfate (position refers are in accordance with RRuff database).

To go further, the XAS spectrum of this sample was carried out at the Pb-L_{III}-edge (**Fig. 4**). Experimental XANES spectrum (**Fig. 4a**) displays a typical white-line at 13044eV followed by a first oscillation centered around 13079eV in agreement with previous studies (*e.g.* Hayes et

al. 2012; Sanderson et al. 2015). The broad shape may be related to the degree of covalent bonding in Pb anglesite as well as the symmetry of Pb(II) sites. The first derivative spectrum displays a peak at 13037 eV, indicative of the 2p → 6d transition in the Pb(II) form.

Even if the purpose of the article is not to make an EXAFS modelling of the anglesite, experimental EXAFS oscillations are shown in **Fig. 4b** and **4c** and the parameters of fit are reported in **Table 3**. RDF curves present a first peak centred at 2Å, related to oxygens atoms surrounding lead. For higher distances, a broad band is evidenced near 4Å. EXAFS spectrum was fitted using backscattering paths extracted from the refined atomic structure determined from XRD. Although anglesite exhibits a low signal/noise ratio for high k values, the simulated curve shows a satisfactory agreement with experimental data, especially for the first coordination shell composed of 12 oxygen atoms.

Finally, the morphology of synthetic anglesite particles has been investigated by SEM and TEM observations as illustrated in **Fig. 5a, 5b, 5c** and **Fig. 5d, 5e, 5f, 5g** respectively. The main type of morphology presenting same chemical analysis (not shown; but in accordance with theoretical structural formula) is sticks-like structure (**Fig. 5a-c**) of about 0.6 to 3µm long (mean 704 nm length from measurement of 25 isolated particles by TEM) with width of approximately 0.1 to 1µm (mean 174 nm width from measurement of 25 isolated particles by TEM). It seems that the crystals are mostly thin to thick tabular probably from crystal structure along the {001}, commonly with {210}, {101} in accordance with the works of Ma et al. (2011) and Stoll (2010). Interestingly, the synthesized anglesite obtained in this study present a polyhedral structure morphology close to those obtained at pH 1.5 reported in the work of Ma et al. (2011). This result strongly suggests the importance of the pH during the synthesis since it has been proposed that increasing the pH of the reaction induces a modification of the crystal shape (Ma et al. 2011).

The TEM morphologies (**Fig. 5d** and **5e**) exhibit particles with poorly defined faces and a length of about 1µm for a width of about 200 nm. It is worth noting the presence of some blocky particles which correspond easily to what has been observed in SEM but of small size.

The SAED plates (**Fig. 5f**) correspond well to an orthorhombic structure in adequacy with the structure of the anglesite. The structural formulae from EDX (**Fig. 5g**) are quite closed to pure anglesite, *i.e.* Pb_1SO_4 and the analysis confirm the purity of sample without the presence of Fe in the structure.

Environmental stability and bioaccessibility of synthetic anglesite

The BCR extraction is used to evaluate the potential environmental stability of anglesite under various physico-chemical conditions traducing a short- and long-term behavior. Indeed, the short term $F_{acid\ soluble}$ mobilizable fraction is nice to understand the behavior of anglesite during rapid condition changes such as rainy episodes relative to the possible exchangeable cationic process. Moreover, the sum of the three first fractions ($F_{acid\ soluble}$ + $F_{reductible}$ + $F_{oxidable}$) is representative of the long-term mobilization, simulating various environmental conditions. The results of the distribution of lead according to BCR sequential extraction protocol are 0.25% (± 0.3%) – 1462 mg/kg (± 53 mg/kg), 0.75% (± 0.25%) – 5440 mg/kg (± 56 mg/kg) and 3% (± 0.3%) – 20195 mg/kg (± 742 mg/kg) for $F_{acid\ soluble}$, $F_{reductible}$ and $F_{oxidable}$ respectively, highlighting that residual fraction is predominant, the long-term mobilization ($F_{acid\ soluble}$ + $F_{reductible}$ + $F_{oxidable}$) no exceed 4% - 27097 mg/kg of the total Pb content, so the main part is found in residual fraction, which is the most stable. Except that the residual fraction, the second dominant fraction is the oxidizable ($F_{oxidable}$) with 3%. Finally, the BCR extractions results highlight a good environmental stability for anglesite with a residual fraction near 96% in accordance with the works of Pascaud et al (2015).

The UBM bioaccessibility results of human gastro-intestinal matrix of anglesite is close to 3% (± 0.3%) - 20100 mg/kg (±2000 mg/kg) of Pb content and 0.45% (± 0.05%) - 2500 mg/kg (± 150 mg/kg) for the gastro-intestinal bioaccessibility one. The behavior of anglesite highlights a decrease of the gastro-intestinal bioaccessibility, traducing that more than 96% of Pb is stable in the gastrointestinal tract. These differences in dissolution can be explained by the difference in pH values and by the ionic strength provided by the salts. These results are in accordance with Ruby et al. (1992) for gastric fluid and traduces the small bioaccessibility of Pb into gastro-intestinal tract which limit the contaminant assimilation. Finally, the long-term mobilization ($F_{acid\ soluble}$ + $F_{reductible}$ + $F_{oxidable}$ from BCR experiments) correspond to the bioaccessible part. This fact can be explained by the increase of pH value during gastro-intestinal phases which dissolves anglesite due to the increases of Pb leaching (higher solubility between pH 5 to 9). As already supposed in other studies (Zárate-Gutiérrez and Lapidus 2014), the precipitation of Pb oxy(hydroxy)des may be possible limiting the concentration of Pb in solution.

Conclusion

In summary, this paper aims to present a new synthesis procedure and a complete physico-chemical analysis of crystalline anglesite. The obtained results indicate that the final product has a good crystallinity refers to XRD sharp peak with a straight spectroscopic signature. But, on the contrary to many other procedures using various reagents and solvents (Na_2SO_4, CS_2,

sodium dodecyl sulfate, hexane), the proposed protocol only requires 2 reagents, lead nitrate and ferric sulfate, short hydrothermal ageing at low temperature, and producing easily interesting mass yield of synthetic anglesite. Structural characterization reveals that the obtained synthetic anglesite can be used as a standard for spectroscopic analysis.

The environmental stability and bioaccessibility of anglesite have been done to evaluate environmental stability of anglesite under various physico-chemical conditions and sanitary risks. This makes it possible to have precise data on a pure phase in order to be able to more easily evaluate and understand the role of anglesite, a ubiquitous mineral in As-polluted sites and soils, when it is mixed with other phases, and thus to better understand the health risks.

Acknowledgment

We acknowledge all the DIFFABS staffs for assistance in using beamline DIFFABS at Soleil Synchrotron, and Pr. M.E.S. Glaoui for his constructive remarks.

Ethics approval and consent to participate

Not applicable.

Consent to Publish

Not applicable.

Authors Contributions

Matthias MONNERON-GYURITS, Emmanuel JOUSSEIN, Alexandra COURTIN-NOMADE, Olivier GRAUBY, Erwan PAINEAU, Solenn REGUER and Marilyne SOUBRAND conceptualized the study, participated in the study design, collected the data and revised the manuscript. All authors read and approved the final manuscript.

Funding

This study was funded by SOLEIL for provision of synchrotron radiation facilities (proposal 20171406), and The Soil Take Care SUDOE program (project UE-16-SOE1/P4/F0023).

Competing interests

The authors declare no competing interests.

Availability of data and materials

Anglesite may be available from the corresponding author on reasonable request.

References

Antao SM (2012) Structural trends for celestite ($SrSO_4$), anglesite ($PbSO_4$), and barite ($BaSO_4$): Confirmation of expected variations within the SO_4 groups. Am Min 97:661–665. https://doi.org/10.2138/am.2012.3905

Auret G, Lopez-Sanchez JF, Sahuquillo A, Rubio R., Davidson CM, Ure AM, Quevauviller P (1999) Improvement of the BCR three step sequential extraction procedure prior to certification of new sediment and soil reference materials. J Environ Monit 1:57-6. https://doi.org/10.1039/A807854H

Ball JW, Nordstrom DK (1991) WATEQ4F – User's manual with revised thermodynamic data base and test cases for calculating speciation of major, trace and redox elements in natural waters, U.S.G.S. Open-File Report 90-129, 1991.

Berthonneau J, Grauby O, Ferrage E, Vallet JM, Bromblet P, Dessandier D, Chaudanson D, Baronnet A (2014) Impact of swelling clays on the spalling decay of building limestones: Insights from X-ray diffraction profile modeling. Eur J Mineral 26:643-656. https://doi.org/10.1127/0935-1221/2014/0026-2393

Blount CW (1974) Synthesis of Barite, Celestite, Anglesite, Witherite, and Strontianite from Aqueous Solutions. Am Min 59:1209-1219.

Boni M, Gilg HA, Aversa G, Balassone G (2003) The "Calamine" of Southwest Sardinia: Geology, Mineralogy, and Stable Isotope Geochemistry of Supergene Zn Mineralization. Econ Geol 98:731–748. https://doi.org/10.2113/gsecongeo.98.4.731

Courtin-Nomade A, Waltzing T, Evrard C, Soubrand M, Lenain JF, Ducloux E, Ghorbel S, Grosbois C, Bril H (2016) Arsenic and lead mobility: From tailing materials to the aqueous compartment. J Appl Geochem 64:10–21. https://doi.org/10.1016/j.apgeochem.2015.11.002

Denys S, Caboche J, Feidt C, Hazebrouck B, Dor F, Dabin C, Floch-Barneaud A, Tack K (2009) Biodisponibilité et bioaccessibilité des métaux et metalloïdes des sols pollués pour la voie orale chez l'homme. Environnement Risques et Santé 8:433–438. https://10.1684/ers.2009.0291

Doebelin N, Kleeberg R (2015) Profex: a graphical user interface for the Rietveld refinement program BGMN. J Appl Crystallogr 48:1573–1580. https://doi.org/10.1107/S1600576715014685

Dutrizac JE, Dinardo O, Kaiman S (1980) Factors affecting lead jarosite formation. Hydrometallurgy 5:305–324. https://doi.org/10.1016/0304-386X(80)90022-5

Farmer VC (1977) Infrared Spectra of Minerals. Mineralogical Society of Great Britain & Ireland, London. https://doi.org/10.1180/mono-4

Forray FL, Smith AML, Drouet C, Navrotsky A, Wright K, Hudson-Edwards KA, Dubbin WE (2010) Synthesis, characterization and thermochemistry of a Pb-jarosite. Geochim Cosmochim Acta 74:215-224. http://dx.doi.org/10.1016/j.gca.2009.09.033

Frau F, Ardau C, Fanfani L (2009) Environmental geochemistry and mineralogy of lead at the old mine area of Baccu Locci (South-East Sardinia, Italy). J Geochem Explor 100:105–115. https://doi.org/10.1016/j.gexplo.2008.01.005

Han B, Xie A, Yu Q, Huang F, Shen Y, Zhu L (2012) Synthesis of $PbSO_4$ crystals by hydrogel template on postprocessing strategy for secondary pollution. Appl Surf Sci 261:623–627. https://doi.org/10.1016/j.apsusc.2012.08.069

Hayes SM, Webb SM, Bargar JR, O'Day PA, Maier RM, Chorover J (2012) Geochemical Weathering Increases Lead Bioaccessibility in Semi-Arid Mine Tailings. Environ Sci Technol 46:5834–5841. https://doi.org/10.1021/es300603s

Jacobsen SD, Smyth JR, Swope RJ, Downs RT (1998) Rigid-body character of the SO4 groups in celestine, anglesite and barite. Canad Mineral 36:1053–1060.

James RW, Wood WA (1925) The crystal structure of barytes, celestine and anglesite. Proc. R. Soc. Lond. A 109:598–620. https://doi.org/10.1098/rspa.1925.0148

Lane MD (2007) Mid-infrared emission spectroscopy of sulfate and sulfate-bearing minerals. Am Min 92:1–18. https://doi.org/10.2138/am.2007.2170

Lee JS, Wang HS, Lizuka Y, Yu SH (2005) Crystal structure and Raman spectral studies of $BaSO_4$-$PbSO_4$ solid solution. Z Kristall 220:1-9. https://doi.org/ 10.1524/zkri.220.1.1.58891

Ma Y, Yang L, Shen Y, Xie A (2011) Morphology control of anglesite microcrystals with polyhedron: Synthesis, growth mechanism, and optical properties. Russ J Phys Chem 85:1454–1464. https://doi.org/10.1134/S0036024411080334

Momma K, Izumi F (2011) VESTA 3 for three-dimensional visualization of crystal, volumetric and morphology data. J Appl Crystallogr 44:1272-1276. https://doi.org/10.1107/S0021889811038970

Mondillo N, Boni M, Balassone G, Villa IM (2014) The Yanque Prospect (Peru): From Polymetallic Zn-Pb Mineralization to a Non sulfide Deposit. Econ Geol 109: 1735–1762. https://doi.org/10.2113/econgeo.109.6.1735

Monneron M, Soubrand M, Joussein E, Courtin-Nomade A, Jubany I, Casas S, Bahi N, Faz A, Gabarron M, Acosta JA, Martinez-Martinez S (2020) Investigating the relationship between speciation and oral/lung bioaccessibility of a highly contaminated tailing: contribution in health risk assessment. Environ Sci Pollut Res 27:40732-40748. https://doi: 10.1007/s11356-020-10074-x.

Pascaud G, Lévêque T, Soubrand M, Boussen S, Joussein E, Dumat C (2014) Environmental and health risk assessment of Pb, Zn, As and Sb in soccer field soils and sediments from mine tailings: solid speciation and bioaccessibility. Environ Sci Pollut Res 21:4254-4264. https:// doi/10.1007/s11356-013-2297-2

Pérez-Cid B, Lavilla I, Bendicho C (1998) Speeding up of a three-stage sequential extraction method for metal speciation using focused ultrasound. Anal Chim Acta 360:35–41. doi: 10.1016/S0003-2670(97)00718-6

Ravel B, Newville M (2005) ATHENA, ARTEMIS, HEPHAESTUS: data analysis for X-ray absorption spectroscopy using IFEFFIT. J Synchrotron Radiat 12:537-541. https://doi.org/10.1107/S0909049505012719

Ruby M, Davis A, Kempton JH, Drexler J, Bergstrom PD (1992) Lead Bioavailability - Dissolution Kinetics under Simulated Gastric Conditions. Environ Sci Technol 26:1242–1248. doi: 10.1021/es50002a614

Sanderson P, Naidu R, Bolan N, Lim JE, Ok YS (2015) Chemical stabilisation of lead in shooting range soils with phosphate and magnesium oxide: Synchrotron investigation. J Hazard Mater 299:395–403. https://doi.org/10.1016/j.jhazmat.2015.06.056

Stoll H (2010) Ion Partitioning in Ambient-Temperature Aqueous Systems. The Mineralogical Society of Great Britain and Ireland.

Wang HR, Lee JS, Yu SC (2001) Synthesis of zoning-free $BaSO_4$-$PbSO_4$ solid solution and its structural characterizations. Z Kristall 217:143-148.

Xiang JH, Yu SH, Geng X, Liu BH, Xu Y (2005) Growth of $PbSO_4$ Single-Crystal Nanorods and Optical Properties by a Microemulsion Approach. Cryst Growth Des 5:1157–1161. https://doi.org/10.1021/cg049630t

Zárate-Gutiérrez IR, Lapidus GT (2014) Anglesite ($PbSO_4$) leaching in citrate solutions. Hydrometallurgy 144–145:124-128. doi.org/10.1016/j.hydromet.2014.02.003

Zeman F (1950) William Withering as a mineralogist: The Story of Witherite. Bull Hist Med 24:530–538.

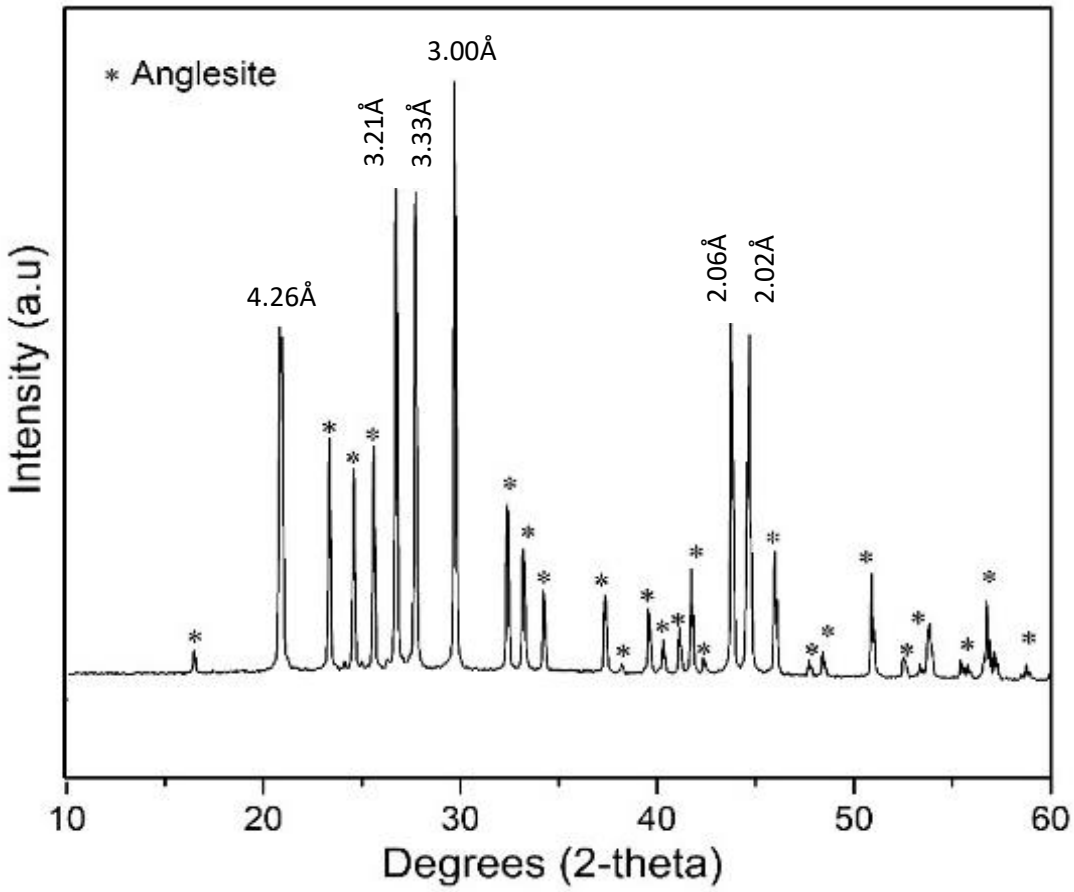

Fig 1 XRD pattern of synthetic anglesite obtained after 24h of hydrothermal treatment. * refer to anglesite diffraction peaks, the position of main reflections are reported in Å.

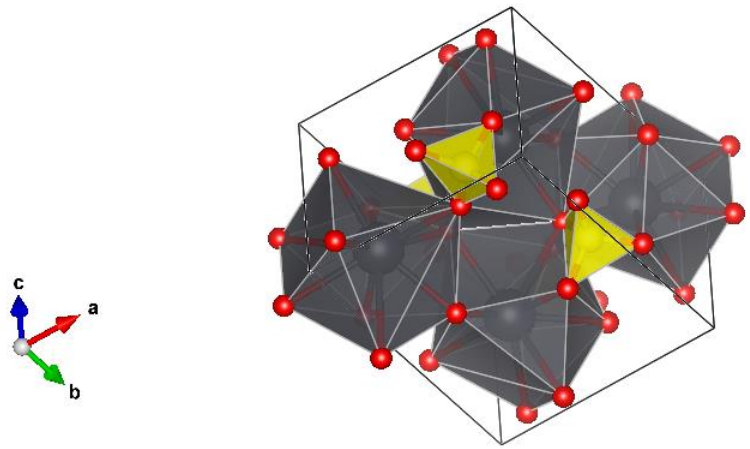

Fig. 2 Structure of synthesized anglesite modelized from Rietveld refinement. Color code: lead (grey); sulfur (yellow); oxygen (red).

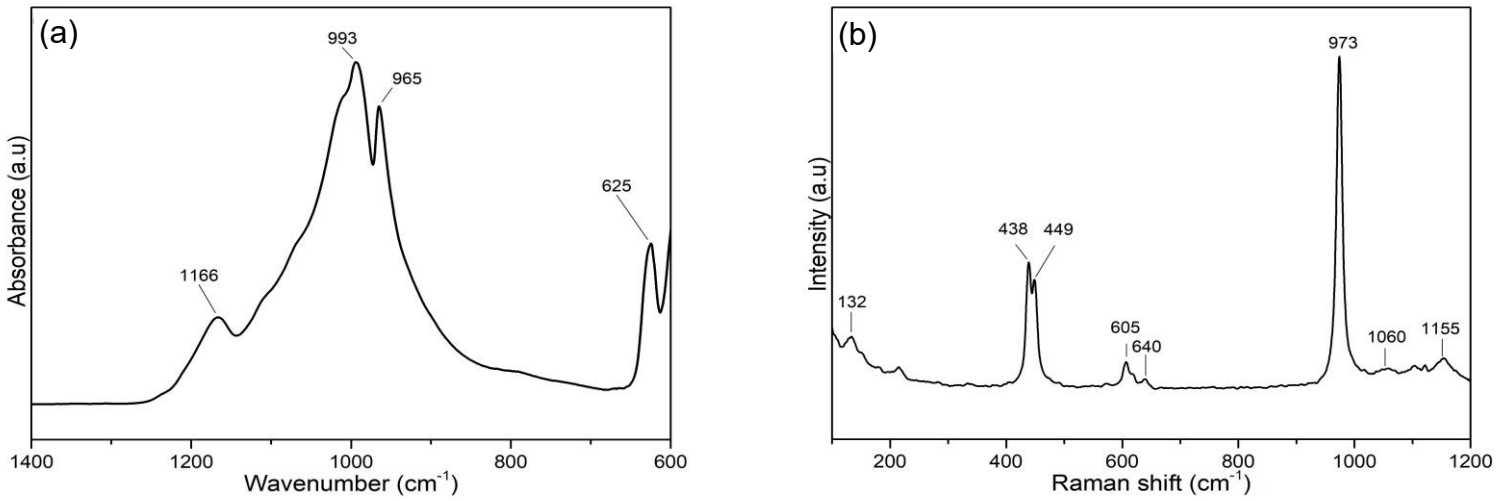

444
445
446 **Fig. 3** Characterization of the synthetic anglesite from (a) Infrared and (b) Raman
447 spectroscopies.

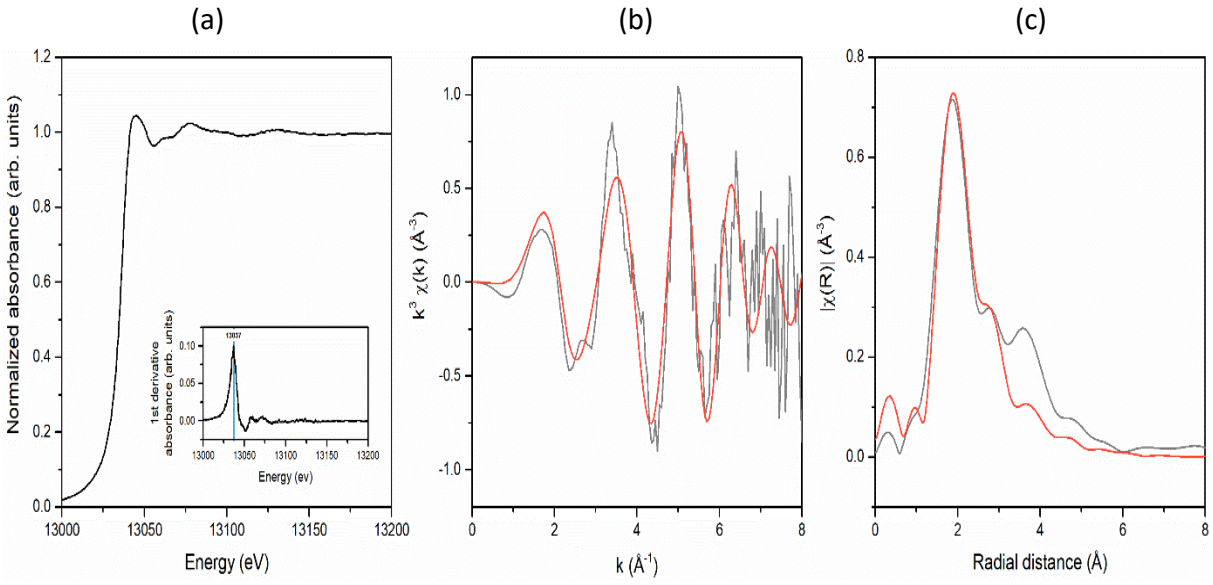

448
449 **Fig. 4** (a) Normalized and first derivative XANES spectra at the Pb-L_{III} edge of the synthetic
450 anglesite obtained after 24h of hydrothermal treatment, (b) Experimental Pb-L_{III} edge EXAFS
451 oscillations, and (c) Radial Distribution Functions (black and red curves refer to experimental
452 and the fitted one from Rietveld refinement data respectively).

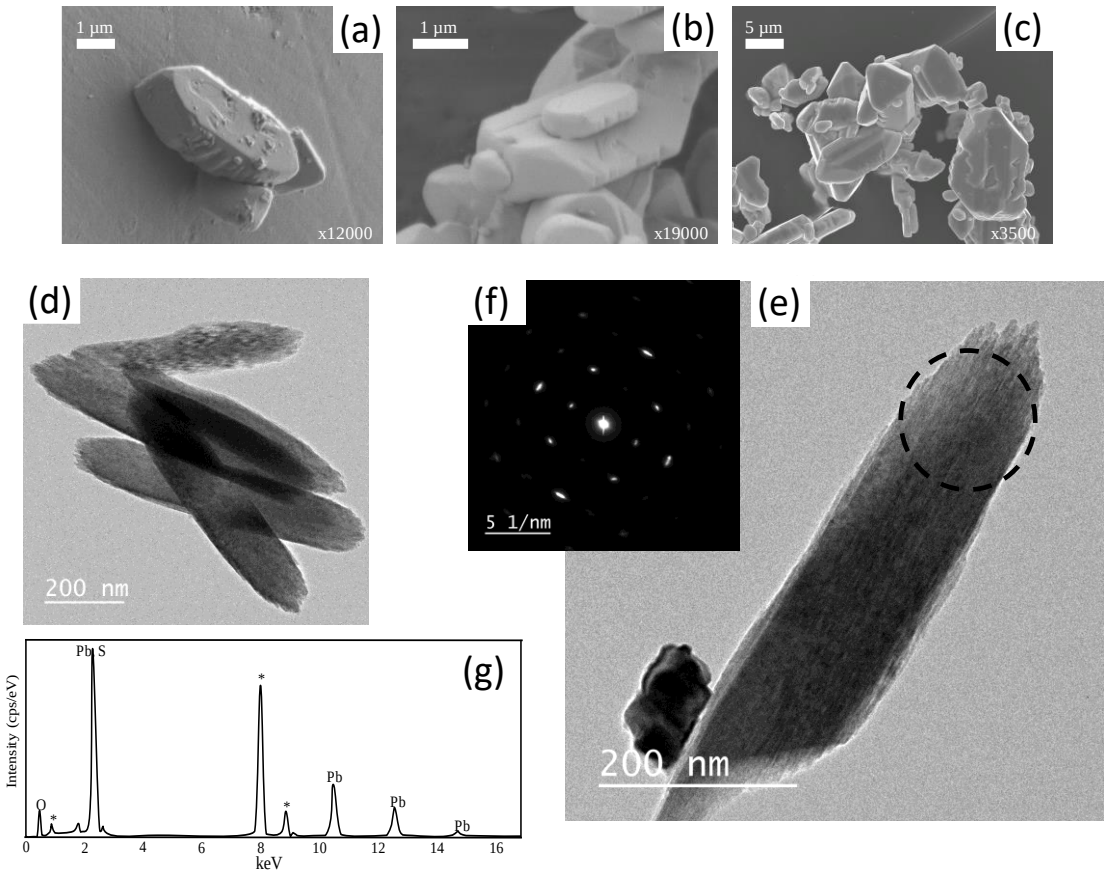

Fig. 5 FEG-SEM images of the synthetic anglesite with different magnifications. (a) and (c) in lower secondary electron (LEI) and (b) in secondary electron in-lens (SEI). TEM images (d, e) of the synthetic anglesite at the same magnifications; (f) selected area electron diffraction (SAED) of the dotted line in (e), and (g) typical Energy Dispersive X-ray analysis on anglesite crystal. The star corresponds to copper grid.

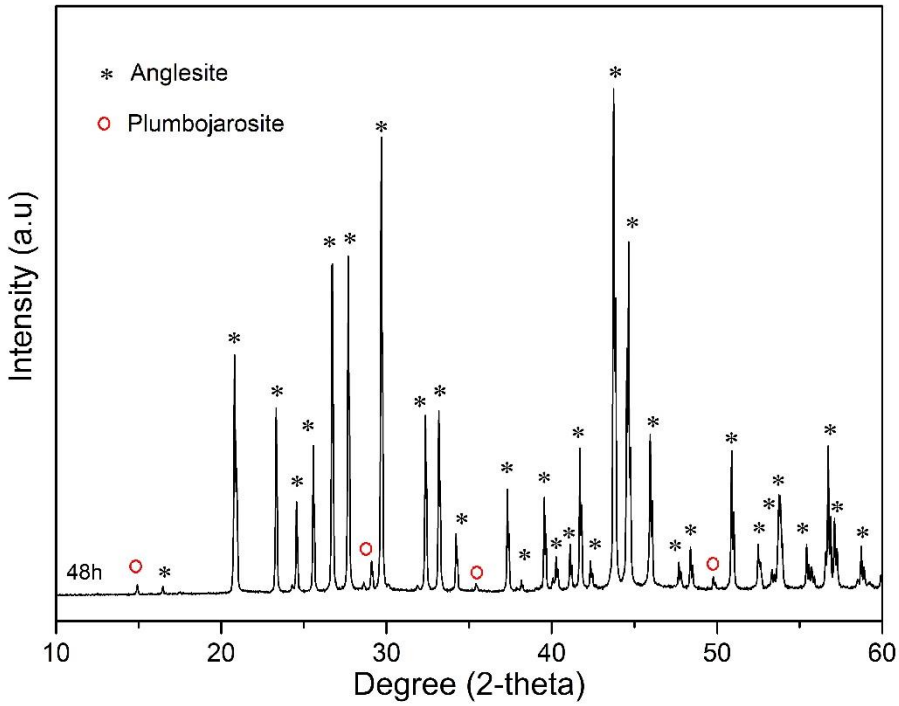

Fig SI 1 XRD pattern of synthetic anglesite obtained after 48h of hydrothermal treatment. The presence of plumbojarosite is effective.

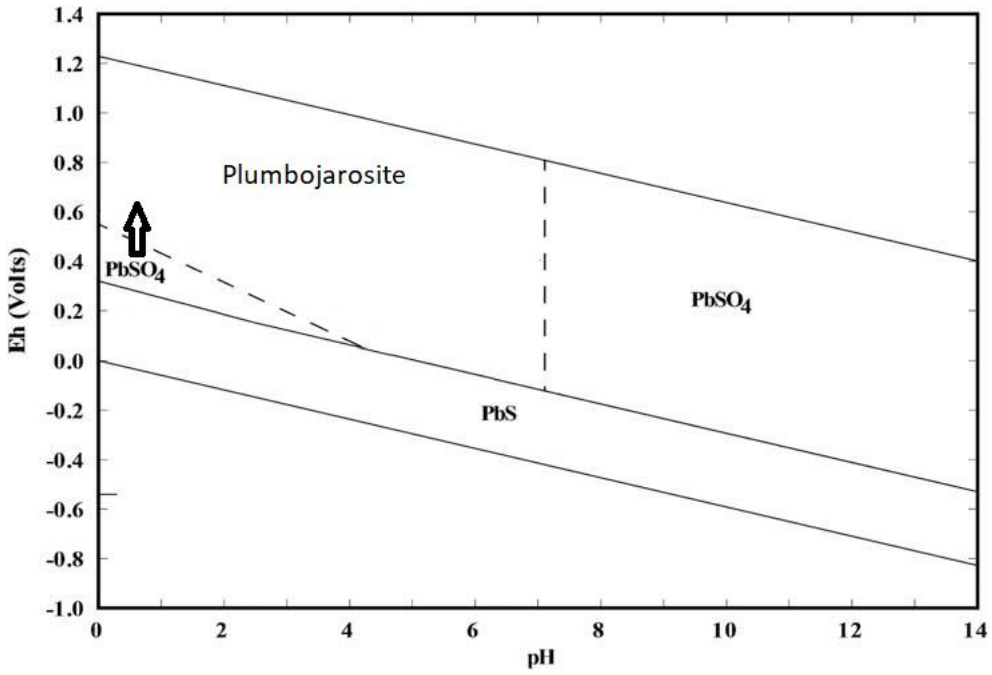

Fig. SI 2 Eh-pH diagram for part of the system S–O–Fe–Pb–H_2O at 25°C adapted from Forray et al. (2010). Note that in the case of this Eh-pH diagram, the assumed activities of dissolved species are 10^{-3} mol/L for S, Fe, and 10^{-8} mol/L for Pb. The arrow traduces the chemical change during time synthesis.

Table 1 Lattice parameters a, b, c (Å) and unit-cell volume (Å^3) determined from Rietveld refinement using BGMN software (angles a = b = c = 90°). Comparison with the literature: data obtained for Antao (2012) are from Aldrich product; Jacobsen et al. (1998) and James & Wood (1925) data after mineral collection, and from Lee et al. (2005) after synthesis.

	a (Å)	b (Å)	c (Å)	V (Å^3)
This study	6.9522	8.4756	5.3980	318.074
Antao 2012	6.95802	8.48024	5.39754	318.486
Jacobsen et al. 1998	6.9549	8.4720	5.3973	318.03
James & Wood 1925	6.93	8.45	5.38	315.0
Lee et al. 2005	6.950	8.475	5.396	317.8

Table 2 Structure parameters determined from Rietveld refinement using BGMN software.

	x	y	z	Occurrence	U
Pb	0.16722	0.18782	0.25000	1.000	0.019
S	0.18370	0.43620	0.75000	1.000	0.008
O1	0.09530	0.59210	0.75000	1.000	0.021
O2	0.04740	0.30720	0.75000	1.000	0.023
O3	0.30900	0.41910	0.97470	1.000	0.015

Table 3 Parameters used to fit the EXAFS spectrum. N is the coordination number, R the radial distance and σ^2 the mean-square variation in path length.

Path index	**Scattering atom(s)**	**N**	**R (radial distance)**	**σ^2 (Å^2)**
1	Pb-O1.1	1	2.58905	0.02183
2	Pb-O2.1	3	2.62643	0.02183
3	Pb-O3.2	2	2.70207	0.02183
4	Pb-O3.3	2	2.89133	0.02183
5	Pb-O2.2	2	2.97481	0.02183
6	Pb-O1.2	2	3.23882	0.02183
7	Pb-S.1	2	3.39596	0.02749

Table SI1. Protocol of the BCR sequential extraction.

Fraction	Chemical reagents	Volume (ml)	Solid–solution ratio (g/ml)	Sonication time and power
F1: acid-soluble/ exchangeable fraction	Acetic acid (CH_3COOH) 0.11 mol/l	20	0.025	20 W for 7 min
F2: reducible fraction	Hydroxylammonium ($HONH_2$ ·HCl) 0.10 mol/l (reagent brought back to pH 2 with nitric acid 69 %)	20	0.025	20 W for 7 min
F3: oxidizable fraction	Hydrogen peroxide (H_2O_2) 30 %	10	0.05	20 W for 2 min
	Ammonium acetate ($C_2H_3O_2NH_4$) 1 mol/l (reagent brought back to pH 2 with nitric acid 69 %)	25	0.02	20 W for 6 min

481
482 Table SI 2. Composition of the digestive solution used during the UBM bioaccessibility
483 test.
484
485

Saliva	Gastric fluid	Bile	Duodenal fluid
KCl 89.6 g/l - 10 mL	NaCl 175.3 g - 15.7 mL	NaCl 175.3 g - 30 mL	NaCl 175.3 g - 40 mL
KSCN 20 g/l - 10 mL	NaH_2PO_4 88.8 g/l - 3 mL	$NaHCO_3$ 84.7 g/l - 68.3 mL	$NaHCO_3$ 84.7 g/l - 40 mL
NaH_2PO_4 88.8 g/l - 10 mL	KCl 89.6 g/l - 9.2 mL	KCl 89.6 g/l - 4.2 mL	KH_2PO_4 8 g/l - 10 mL
NaCl 175.3 g/l - 1.7 mL	$CaCl_2.2H_2O$ 22.2 g /l - 18 mL	HCl 37% g/g - 200 µL	KCl 89.6 g/l - 6.3 mL
NaOH 40 g/l - 1.8 mL	NH_4Cl 30.6 g/l - 10 mL	urea 25 g/l - 10 mL	$MgCl_2$ 5 g/l - 10 mL
urea 25 g/l - 8 mL	HCl 37% g/g - 8.3 mL	$CaCl_2.2H_2O$ 22.2 g/l - 10 mL	HCl 37% g/g - 180 µL
α-Amylase - 145 mg	Glucose 65 g/l - 10 mL	Bovine albumine - 1 g	$CaCl_2.2H_2O$ 22.2 g/l - 9 mL
Uric acid - 15 mg	Glucoronic acid 2 g/l - 10 mL	Porcine bile	Bovine albumine - 1 g
Mucin - 50 mg	Urea 25 g/l - 3.4 mL		Pancreatin - 3 g
	Glucosonamine hydrochlorite 33 g/l - 10 mL		Lipase - 0.5 g
	Bovine albumine - 1 g		
	Pepsin - 1 g		

← *Gastric phase* →
Gastro-intestinal phase ←

486
487
488